LANGMUIR

pubs.acs.org/Langmuir Article

# Evaporative Deposition of Surfactant-Laden Nanofluid Droplets over a Silicon Surface

Xiao-Ye Yang, Guo-Hao Li, Xianfu Huang, and Ying-Song Yu*

Cite This: *Langmuir* 2022, 38, 11666−11674 Read Online

ACCESS | Metrics & More | Article Recommendations | Supporting Information

**ABSTRACT:** Morphologies of evaporative deposition, which has been widely applied in potential fields, were induced by the competition between internal flows inside evaporating droplets. Controlling the pattern of deposition and suppressing the coffee-ring effect are essential issues of intense interest in the aspects of industrial technologies and scientific applications. Here, evaporative deposition of surfactant-laden nanofluid droplets over silicon was experimentally investigated. A ring-like deposition was formed after complete evaporation of sodium dodecyl sulfate (SDS)-laden nanofluid droplets with an initial SDS concentration ranging from 0 to 1.5 CMC. In the case of initial SDS concentrations above 1.3 CMC, no cracks were observed in the ring-like deposition, indicating that the deposition patterns of nanofluid droplets could be completely changed and cracks could be eliminated by sufficient addition of SDS. With the increase of the initial concentration of hexadecyl trimethylammonium bromide (CTAB), the width of the deposition ring gradually decreased until no ring-like structure was formed. On the contrary, with the increase of the initial Triton X-100 (TX-100) concentration, the width of the deposition ring gradually increased until a uniform deposition was generated. Moreover, when the initial TX-100 concentration was high, a "tree-ring-like" pattern was discovered. Besides, morphologies of evaporative pattern due to the addition of surfacants were qualitatively analyzed.

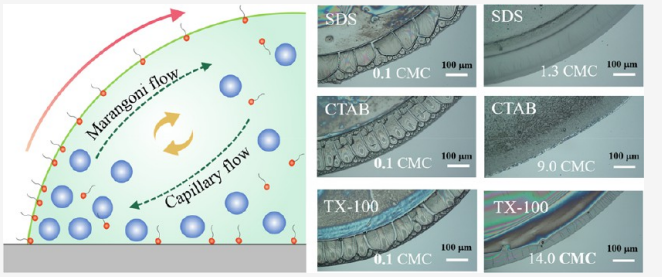




## INTRODUCTION

When a droplet containing nonvolatile micro/nanoparticles completely evaporates on a solid surface, these particles will deposit on the surface and various deposition patterns will be formed. Evaporative deposition pattern may be strongly influenced by internal flows such as outward capillary flow toward the contact line caused by higher evaporation rate near the edge of the droplet[1] and Marangoni flow induced by the gradient of surface tension caused by the gradients of temperature[2,3] or concentration[3] inside the droplet. On account of the existence of capillary flow, a universal ring-shaped deposition pattern is generated. There is a tendency to regulate and control the evaporative deposition pattern of a sessile droplet containing particles for its wide application in many fields including ink-printing,[4−7] coating technology,[8,9] medical diagnosis,[10,11] biomedicine,[12] DNA/RNA mapping,[13,14] and nanomaterial fabrication.[15−17]

Indeed, a variety of strategies have been proposed for suppressing or controlling the coffee ring effect. Three physical strategies—(i) avoiding the contact line being pinned, (ii) disturbing the outward capillary flow, (iii) thwarting particles being transported to the edge of sessile droplets—were enumerated for suppressing the coffee ring effect.[18] On a micropatterned hydrophobic or superhydrophobic surface, droplets may be at a Cassie or Wenzel wetting state, leading to the difference in evaporative deposition.[19,20] Eral et al.[21] provided a method of applying an electric field to evaporating droplets to obtain a homogeneous deposition. Changing the pH of evaporating droplets was found to effectively suppress the coffee ring effect.[22] Furthermore, substrate temperature[23,24] and evaporative environment[25] were approved factors for preventing the coffee ring effect. Moreover, adding some amount of polymer additives[26] was also found to be effective for the strong Marangoni flow inside evaporating droplets.

However, there is an intense interest in exploring applicable strategies for inducing internal flows inside an evaporating droplet. Surfactant, containing one or more hydrophobic tails and a hydrophilic headgroup, can dramatically change the flow of evaporating fluid which was triggered by changes in surface properties,[27] evaporation rate,[28] and surface tension[29] of a droplet resulting from the adsorption of surfactant molecules at the liquid−vapor interface. Additionally, the surface tension of surfactant solutions would never change distinctly when the concentrations are above the critical micelle concentration (CMC). Therefore, an enlightenment of employing surfactants

**Received:** June 15, 2022
**Revised:** August 31, 2022
**Published:** September 13, 2022





https://doi.org/10.1021/acs.langmuir.2c01564
*Langmuir* 2022, 38, 11666−11674

for controlling the final deposition was generated. In this regard, the Marangoni vortex could be instigated by adding anionic surfactants such as sodium dodecyl sulfate (SDS),[30] resulting in the uniform deposition of colloidal particles after complete evaporation. As demonstrated, hexadecyl trimethylammonium bromide (CTAB)—a kind of a cationic surfactant—played an important role in eliminating the coffee ring effect, which was conducive to Marangoni flow, and eventually had a homogeneous deposition.[31] Also, there was proof that the coffee ring effect could be altered with the addition of Triton X-100 (TX-100), a nonionic surfactant.[32] However, to our best knowledge, the combined effect of surfactant type and surfactant concentration on evaporative deposition has never been reported up until now.

In this paper, different categories and concentrations of surfactants were selected, and evaporative deposition of surfactant-laden nanofluid droplets over the silicon surface was experimentally investigated. It was found that the types and concentrations of the surfactant had an enormous influence on the morphologies of evaporative deposition. SDS concentration also has a great influence on apparent crack (particle separation) morphologies and can even eliminate cracks when it is just greater to some extent than 1.0 CMC; homogeneous patterns were achieved when the initial concentrations of CTAB and TX-100 were relatively high.

## MATERIALS AND METHODS

Prepolished silicon wafers (Tebo Technology Co., Ltd., China) were ultrasonically cleaned by acetone and ethanol successively for 15 min. Three kinds of surfactants—SDS [Chemical Reagent, Aladdin, ≥99.0% (GC), China], CTAB [Bio-Reagent, Sigma-Aldrich, ≥99.0% (GC), India], and TX-100 [Chemical Reagent, Aladdin, ≥99.0% (GC), China]—were selected for preparing suspensions with different concentrations, respectively. Surfactant-laden nanofluids were obtained by diluting PS nanoparticle[33] suspension with an initial mass percent of 10.06 wt % (PS02N, mean diameter: 44 nm, Bangs Laboratory, USA) with deionized water and surfactant solutions. In the surfactant-laden nanofluid solutions containing only one kind of surfactant, the mass fraction percent of PS nanoparticles was fixed at 0.64 wt % and surfactant concentration was in different ranges as follows: (i) the SDS concentration ranged from 0.1 to 1.5 CMC (1 CMC = 8.2 mM[34]); (ii) the CTAB concentration ranged from 0.1 to 9.0 CMC (1 CMC = 0.92 mM[35]); (iii) the TX-100 concentration ranged from 0.1 to 18 CMC (1 CMC = 0.24 mM[36]). All of the surfactant-laden nanofluid solutions were ultrasonically stirred for 15 min to ensure the uniform distribution of nanoparticles and used within 24 h.

Surfactant-laden nanofluid droplets with a nominal volume of 0.8 $\mu$L were extracted with a micropipette and gently dropped on the silicon surface. Meanwhile, mixture droplets were observed with a three-dimensional digital microscope (KH-8700, Hirox, Japan) from the top view at 1 fps. The ambient temperature and relative humidity were 25 ± 1 °C and 47 ± 5%, respectively. Each experiment was repeated at least four times to ensure its reproductivity. It should be noted that surfacant molecules will form micelles above 1 CMC and the distribution of micelles in the evaporative deposition might be analyzed using energy dispersive X-ray spectroscopy.[37]

## RESULTS AND DISCUSSION

**1. Morphology and Evolution of Apparent Cracks in the Evaporation of SDS-Laden Nanofluid Droplets.** Figure 1 shows the apparent, advancing, and receding contact angles of SDS droplets on silicon, which were represented by $\theta_e$, $\theta_a$, and $\theta_r$, respectively. It was found that the values of $\theta_e$, $\theta_a$, and $\theta_r$ all decreased with increasing SDS concentration when it was less than 1.0 CMC. However, they remained nearly unchanged when the concentration was greater than 1.0 CMC.

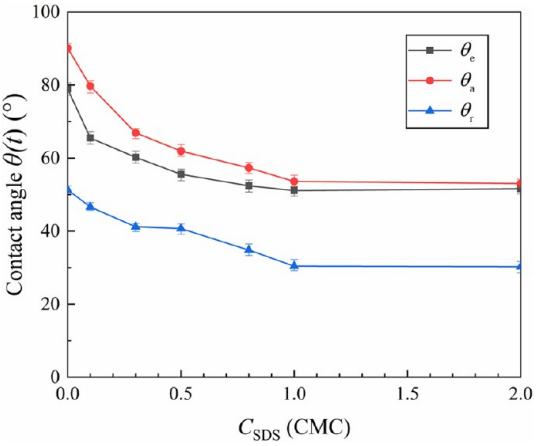


**Figure 1.** Contact angle of SDS droplets on the silicon surface.

Figure 2 shows the evaporative deposition of SDS-laden nanofluid droplets with initial SDS concentrations ranging from 0.1 to 1.5 CMC (evaporation curves of SDS-laden nanofluid droplets are given in Figure S2, and the height profile of some evaporative depositions is given in Figure S8). A previous study[38] demonstrated that periodic radial cracks were developed in the evaporative deposition of nanofluid droplets without the addition of SDS molecules. When SDS molecules was introduced into nanofluid droplets, deposition patterns with different morphologies of cracks were obtained. When the initial SDS concentration ranged from 0.1 to 0.8 CMC, complex, diverse, nonuniform, and nonperiodic morphologies of cracks were observed. When the initial SDS concentration was 0.9 CMC, periodic radial cracks were found. When the initial SDS concentration was in the range from 1.0 to 1.2 CMC, only a few cracks were formed in part of the evaporative deposition. Note that no cracks were observed when the initial SDS concentration was 1.3 or 1.5 CMC.

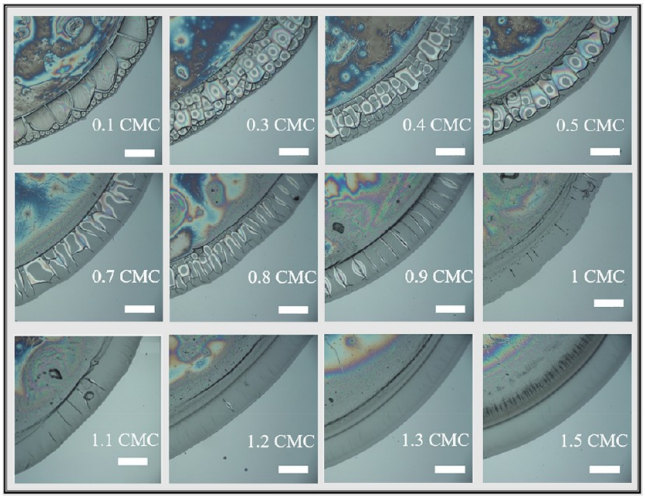


**Figure 2.** Deposition patterns of PS nanofluid droplets laden with different concentrations of SDS. Scale bars: 100 $\mu$m.

The evolution of apparent cracks during the evaporation of SDS-laden nanofluid droplets with initial SDS concentrations ranging from 0.1 to 1.2 CMC was shown in Figure 3. It has



https://doi.org/10.1021/acs.langmuir.2c01564
Langmuir 2022, 38, 11666−11674

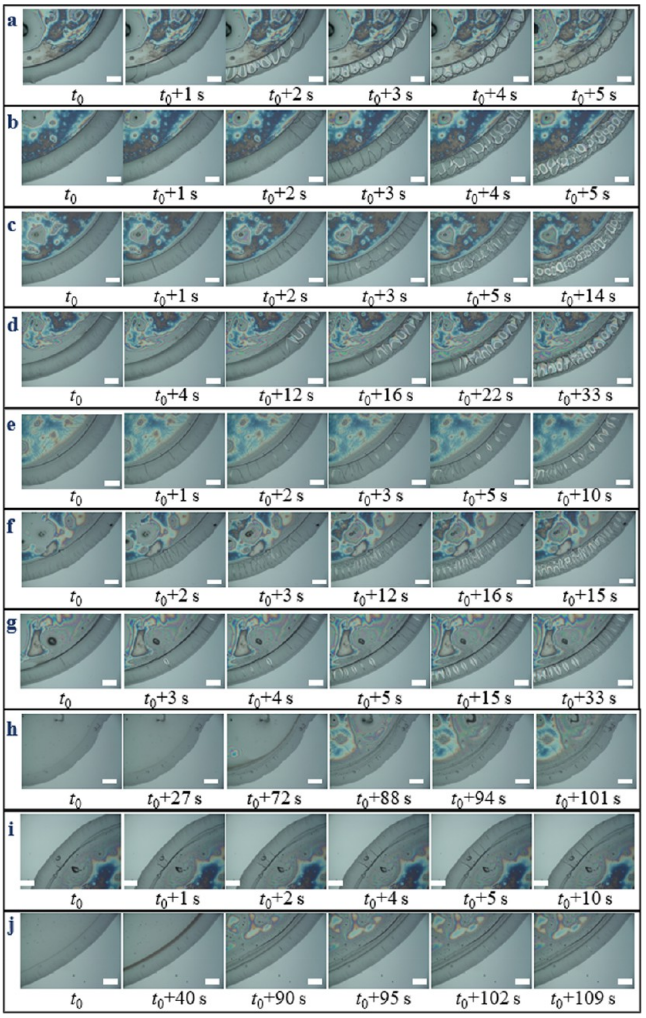


**Figure 3.** Evolution of apparent cracks during the evaporation of SDS-laden nanofluid droplets. Parts a−j represent the initial SDS concentration of 0.1−1.2 CMC, respectively. The time $t_0$ denotes the instant just before the formation of the first apparent crack. Scale bars: 100 $\mu$m.

been widely accepted that crack formation is induced by capillary force.[39−43] With the loss of a lot of solvent, there would a thin liquid film covering the clustered nanoparticles. Capillary force between nanoparticles increases greatly with the film becoming thinner and thinner, leading to the increase in stress.[39] Under the action of the capillary force, adjacent particles would be more likely pulled apart, resulting in the formation of cracks. From the viewpoint of energy, the thin liquid film covering the surface of the sediments at the final stage of evaporation tries to expand,[44] thus more and more energy could be accumulated by reducing the stress in the process. However, silicon is a hard substrate and the bottom of the thin film expanded to the substrate until it adhered completely, avoiding the production of stress relaxation.[44] While on the top of the thin film, the stress could be released in the surface of the sediments by producing cracks.

A theoretical model was developed here to elucidate the formation of evaporative deposition, as shown in Figure 4. During the process of crack formation, two types of capillary forces existed, viz., the lateral capillary force $F_{LC}$ and the normal capillary force $F_{NC}$. The lateral capillary force tends to attract nanoparticles and bring them together, while the normal capillary force tends to adhere nanoparticles to the solid surface, as shown in Figure 4a. $F_{LC}$ was expressed as[45,46]

$$F_{LC} = \pi\gamma_{lv}(r_1 \sin\phi)^2/L \quad (1)$$

where $r_1$ is the radial distance of the liquid film covering the particle surface, $\phi$ is the meniscus slope angle, and $L$ is the center-to-center spacing, as shown in Figure 4a.[47] It should be noted that eq 1 is valid when the ratio of the center-to-center spacing to capillary length $l_C$ ($l_C = \sqrt{\frac{\gamma_{lv}}{\rho g}}$, where $\rho$ and $g$ are the density of the liquid and the gravitational acceleration, respectively) is far less than 1.[47]

$F_{NC}$ was given as[45,47]

$$F_{NC} = \pi r_1 \gamma_{lv} \sin\phi \quad (2)$$

Besides, the particles were also under the action of friction from the substrate which was expressed as[48]

$$F_f = \overline{n} f F_a \quad (3)$$

where $\overline{n}$ is the equivalent number of particles arrayed as a line, $f$ is the friction coefficient taking into account the influence of the liquid layer between nanoparticles and the substrate based on the lubrication theory,[49,50] and $F_a$ is the total adhesive force including gravity, electrostatic force, van der Waals force, and the normal capillary force.[51] Compared with the normal capillary force, the other three forces could be neglected;[48] thus, $F_a$ was approximately equal to $F_{NC}$. When $F_f \geq F_{LC}$, the movement of particles inside the droplet would be prevented. When $r_1$ and $\phi$ reached the corresponding extreme values, viz., $r_1 = R$ and $\phi = 90°$, the liquid film would disappear. Hence, the number of particles to keep particles pinned in the fluid could be derived from eqs 1−3

$$\overline{n} \geq \frac{R}{Lf} \quad (4)$$

where $R$ is the radius of a nanoparticle. Equation 4 indicated that there was a negative correlation between $\overline{n}$ and $L$. As the circumferential crack width decreased, the center-to-center spacing in the circumferential direction $L_c$ became shorter with increasing initial SDS concentration, as shown in Figure 2.

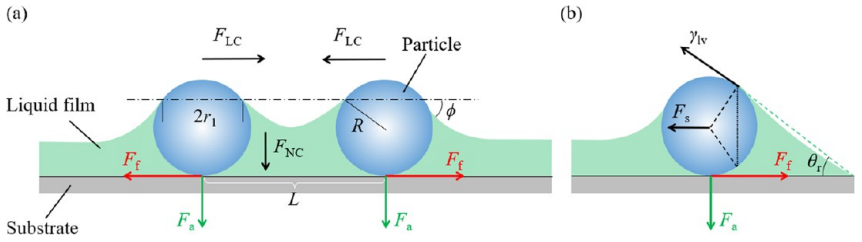


**Figure 4.** Schematics of the mechanism for particles in different regions: (a) particles inside the droplet; (b) particles adjacent to the contact line.



https://doi.org/10.1021/acs.langmuir.2c01564
Langmuir 2022, 38, 11666−11674

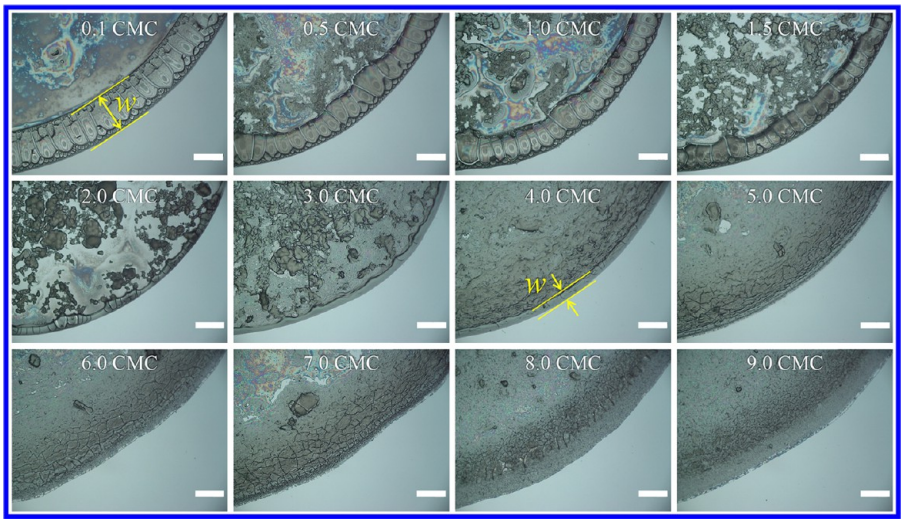


**Figure 5.** Deposition patterns of CTAB-laden PS nanoparticle droplets with different concentrations. Scale bars: 100 $\mu$m.

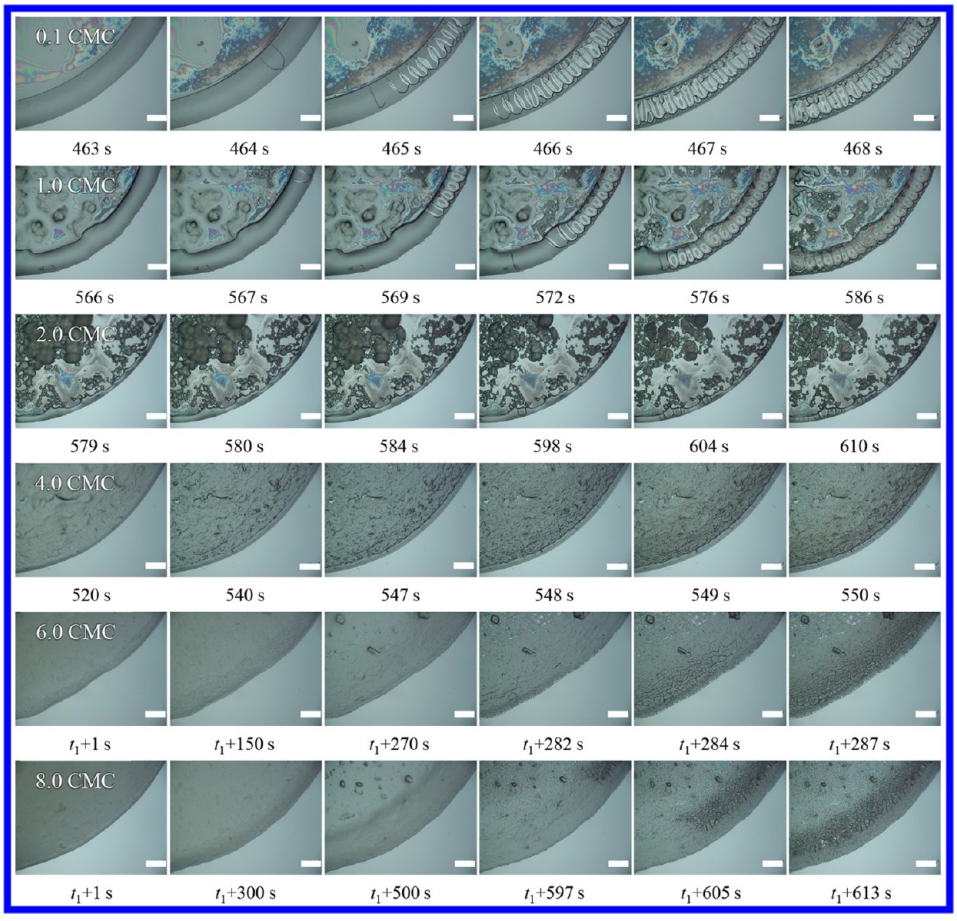


**Figure 6.** Evolution of deposition patterns during the evaporation of CTAB-laden nanoparticle droplets. The time $t_1$ denoted the instant just before the formation of the deposition patterns. Scale bars: 100 $\mu$m.

Thus, $\overline{n}$ would get larger and the number of nanoparticles gathered in the circumferential direction would increase, implying there would be fewer cracks (0.1−0.8 CMC) until no crack (0.9−1.5 CMC) along the circumferential direction as the initial SDS concentration increased.

Particles adjacent to the contact line also experience the surface tension force $F_s$ exerted by the liquid−air interface at the edge of the liquid film, as shown in Figure 4b. $F_s$ could be expressed as[52]

$$F_s = 2\pi R\gamma_{lv} \cos \theta_r \tag{5}$$

When $F_f \geq F_s$, the movement of nanoparticles toward the contact line would be suppressed. Thus, the number of particles for the pinning of nanoparticles could be derived by combining eqs 2 and 3 with eq 5 and expressed as



https://doi.org/10.1021/acs.langmuir.2c01564
Langmuir 2022, 38, 11666−11674

$$\overline{n} \geq \frac{\cos \theta_r}{f} \tag{6}$$

From eq 6, there was a positive correlation between $\overline{n}$ and $\cos \theta_r$. As shown in Figure 1, $\theta_r$ got smaller with the increase of SDS concentration until it was kept unchanged above 1 CMC. Thus, $\overline{n}$ would get larger and the number of particles gathered in the contact line would increase, indicating that there were fewer cracks (0.1−0.4 CMC) until no crack (0.5−1.5 CMC) around the region of the contact line.

Because $\theta_r$ was more sensitive to SDS concentration than $L$, according to eqs 5 and 6, the equivalent particles accumulated earlier near the contact line than inside the droplet, contributing to the disappearance of cracks on the edge of the deposition. From Figure 2, it was easily found that the circumferential cracks disappeared, and only periodic radial cracks were formed on the surface of the deposition when the initial SDS concentration was in the range from 0.9 to 1.2 CMC. It was worth noting that the number of radial cracks increased (0.1−0.8 CMC) as the center-to-center spacing in the radial direction $L_r$ decreased. In order to eliminate the marginal and circumferential cracks, more particles were required to congregate there, resulting in fewer particles accumulating along the radial direction. In that way, it was difficult for the particles to be arrayed along the radial direction to reach the equilibrium state; thus, more radial cracks were generated. At a relatively high SDS concentration (1.0−1.2 CMC), the average center-to-center spacing $L_r$ in the radial direction decreased, resulting in the decrease of the number of radial cracks. Hence, only radial cracks were discovered in part of the circular sediments. When the initial SDS concentration was high (1.3−1.5 CMC), there was much stronger Marangoni flow[30,53] and SDS molecules would be transported to the interior, leading to the reduction in the local liquid−vapor interfacial tension. Thus, the capillary stress would be much less and could not induce enough tensile stress[54] for the cracking of the thin film.

**2. Morphology and Evolution of Apparent Cracks in the Evaporation of CTAB-Laden Nanofluid Droplets.** Figure 5 shows the deposition pattern of CTAB-laden PS nanofluid droplets with different concentrations (evaporation curves of CTAB-laden nanofluid droplets are given in Figure S4, and the height profile of some evaporative depositions is given in Figure S9). When the initial CTAB concentration was in the range from 0.1 to 4.0 CMC, periodic radial cracks were formed on the deposition pattern. With the increase of the initial CTAB concentration, the number of cracks generally decreased, and more nanoparticles were deposited on the interior. More importantly, the width of the deposition ring gradually decreased. When the initial CTAB concentration ranged from 5.0 to 9.0 CMC, the deposition ring disappeared and a uniform deposition was obviously formed with cracks near the edge of the deposition.

The evolution of deposition patterns during the evaporation of CTAB-laden nanofluid droplets with initial CTAB concentrations ranging from 0.1 to 9.0 CMC was shown in Figure 6. Assuming that a droplet has a spherical cap and the contact angle is less than 90°, a scaling law related to the width of the coffee ring was proposed as follows[55]

$$w/R_d \sim \sqrt{\psi} \tag{7}$$

where $w$ is the width of the coffee ring, $R_d$ is the radius of the deposition, and $\psi$ is the initial volume fraction of the particles; in our experiment, $\psi$ is a constant. Hence, there is a negative correlation between the width of the coffee ring and the radius of the deposition.

Generally speaking, the competition between flows inside the droplet would determine the morphology of deposition. Inside an evaporating sessile droplet, there are usually two kinds of flows, viz., the capillary compensatory flow caused by contact-line pinning[1] and the Marangoni flow induced by the gradient of surface tension,[30,53] as shown in Figure 7. When

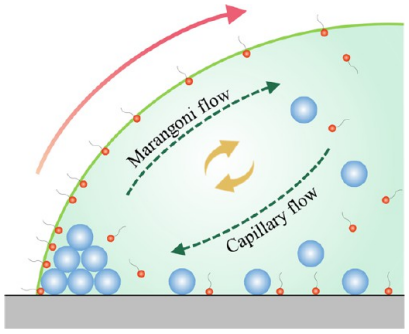


**Figure 7.** Diagram of internal flows inside evaporating CTAB-laden nanoparticle droplets.

the initial CTAB concentration was in the range from 5.0 to 9.0 CMC, particles would be pulled from the edge to the interior of the droplet due to the dominant Marangoni flow, the ring-shaped structure would disappear, and the homogeneous deposition pattern would be generated.

**3. Morphology and Evolution of Apparent Cracks in the Evaporation of TX-100-Laden Nanofluid Droplets.** Figure 8 shows the deposition pattern of TX-100-laden nanofluid droplets with different initial TX-100 concentrations (evaporation curves of TX-100-laden nanofluid droplets are given in Figure S6, and the height profile of some evaporative depositions is given in Figure S10). The circular width gradually increased with the increase of initial TX-100 concentration, which indicated the internal deposition was significantly formed. Furthermore, the number of cracks increased and the width of the cracks decreased distinctly. The cracks gradually expanded inward when the initial TX-100 concentration ranged from 0.1 to 12.0 CMC. Interestingly, when the initial TX-100 concentration was relatively high (14.0−18.0 CMC), a "tree-ring-like" structure was discovered on the deposition. The evolution of deposition patterns during the evaporation of TX-100-laden nanofluid droplets with initial CTAB concentrations ranging from 0.7 to 14.0 CMC was shown in Figure 9.

Actually, cracks are formed as a result of competition between the capillary force and the friction force. From Figure 9, it was found that the average width of cracks decreased with increasing initial TX-100 concentration when the concentration ranged from 0.1 to 12.0 CMC, which demonstrated more equivalent nanoparticles were required to reach the equilibrium state from eq 4, while nanoparticles in the whole zone were lacking to keep them pinned along with extended inward deposition. Thus, denser cracks were generated with increasing initial TX-100 concentration.

When the contact line was initially pinned, the nanoparticles and TX-100 molecules were transported to the edge of the droplet due to the outward capillary flow. TX-100 molecules aggregated at the liquid−vapor interface near the contact line


https://doi.org/10.1021/acs.langmuir.2c01564
Langmuir 2022, 38, 11666−11674

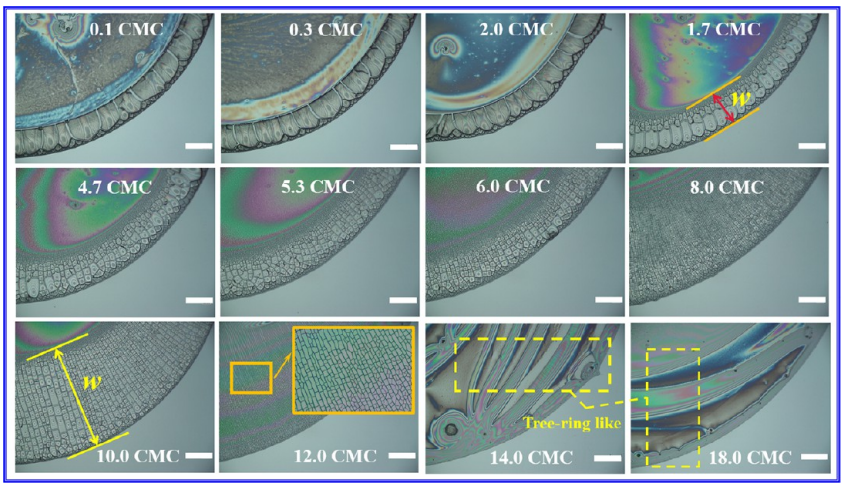


**Figure 8.** Deposition patterns of TX-100 containing PS nanoparticle droplets with different concentrations. Scale bars: 100 $\mu$m.

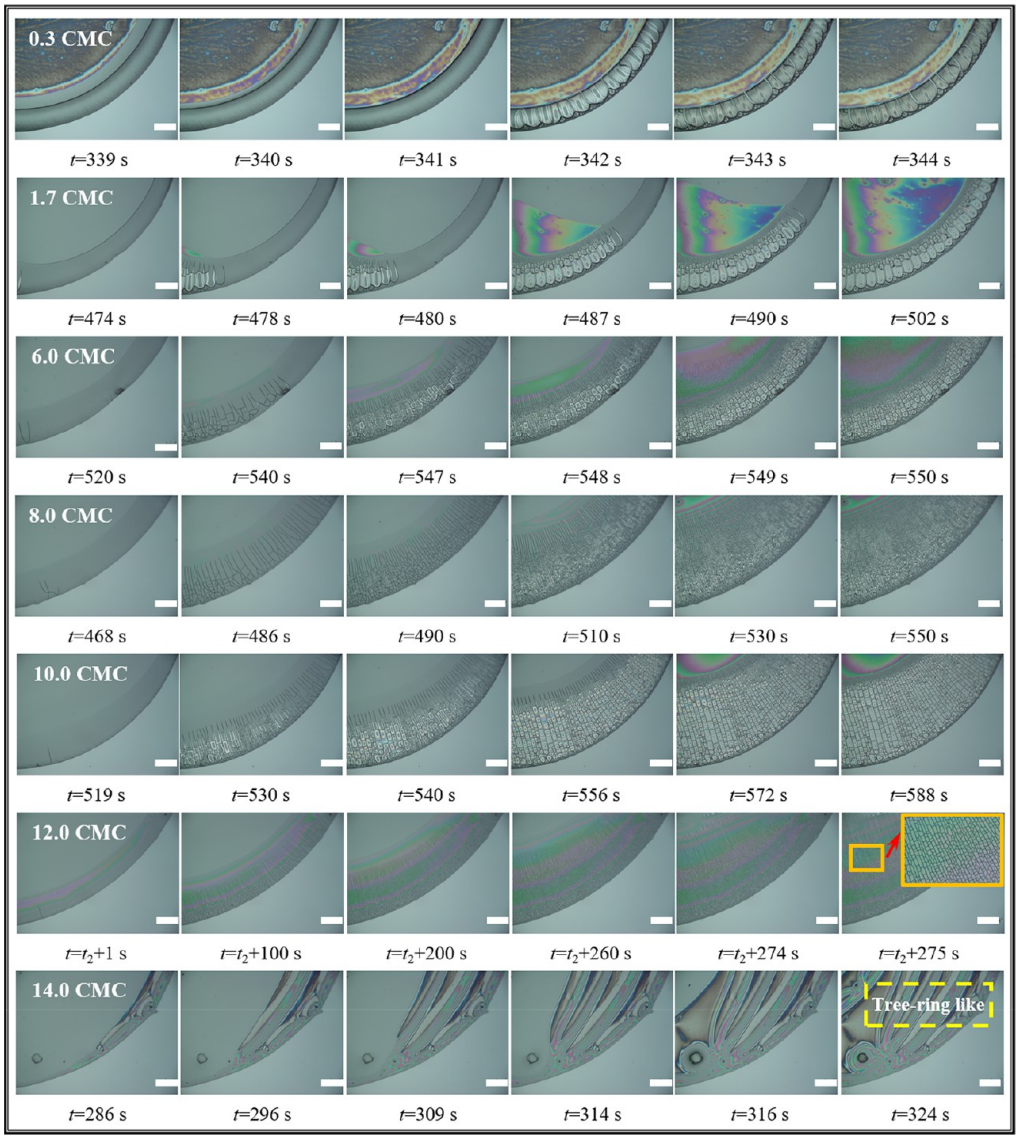


**Figure 9.** Evolution of deposition patterns during the evaporation of TX-100-laden nanoparticle droplets. The time $t_2$ denotes the instant just before the formation of the deposition patterns. Scale bars: 100 $\mu$m.



https://doi.org/10.1021/acs.langmuir.2c01564
Langmuir 2022, 38, 11666−11674

locally reduced the liquid−vapor interfacial tension. Thus, Marangoni flow was induced by the gradient of surface tension. When Marangoni flow was strong enough to carry a large number of nanoparticles and TX-100 molecules toward the center of the droplet, the contact line was depinned. However, when the local concentration of TX-100 was high, the induced Marangoni flow was weaker; thus, nanoparticles were pulled from the droplet center to the contact line due to the dominant capillary flow because of the pinning of the contact line. Subsequently, Marangoni flow restarted, and the process was repeated, as shown in Figure 10. As a result, a "tree-ring-like" structure of nanoparticles was formed during the recurrent transition between the pinning and the depinning of the contact line. Therefore, when the contact line was ultimately depinned, the remaining nanoparticles were deposited in the center as the contact line moved, resulting in a nearly uniform evaporative deposition.

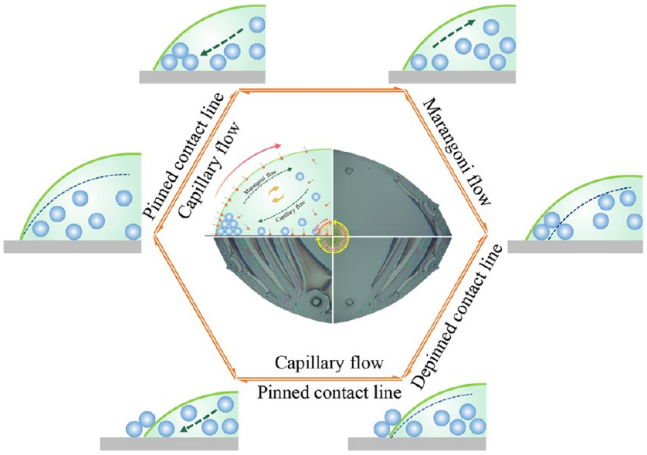


**Figure 10.** Schematic diagram of the formation of a "tree-ring-like" structure.

Besides, it should be noted that, though different surfactants and different surfactant concentrations were chosen to study their combined effect on the evaporative deposition of nanoparticles, all surfactants influence the morphology in the same way, as shown in Figure 7.

## CONCLUSIONS

Evaporative deposition of surfactant-laden nanofluid droplets over a silicon surface was experimentally studied. The following was found: (i) The addition of SDS molecules into nanofluid droplets was found to have an obvious influence on the formation of cracks. Moreover, cracks could be completely eliminated at an initial SDS concentration above a critical value. Moreover, a theoretical model taking capillary force, friction between nanoparticles and the substrate in a fluid, as well as the surface tension force into account was developed to elucidate the formation of cracks. (ii) The width of the deposition ring gradually decreased until it disappeared with the increase of initial CTAB concentration. In the case of high initial CTAB concentrations, a relatively homogeneous deposition was formed. (iii) With the increase of the initial TX-100 concentration, the width of the deposition ring gradually increased until the deposition was completely uniform, and the number of cracks gradually increased. Moreover, a "tree-ring-like" pattern was discovered for the case of high initial TX-100 concentrations (14.0−18.0 CMC). In summary, morphologies of deposition could be influenced by adding surfactant into droplets. Hence, this work provides a useful and reliable method to fulfill regulation of the particle deposition pattern, which may open up deeper application prospects for particle self-assembly, coating, and nanomaterial technology.

## ASSOCIATED CONTENT

### Supporting Information

The Supporting Information is available free of charge at https://pubs.acs.org/doi/10.1021/acs.langmuir.2c01564.

Surface tensions of surfactant solutions, evaporative dynamics of surfactant-laden nanofluid droplets on a silicon surface, and characterization of evaporative deposition (PDF)

## AUTHOR INFORMATION

### Corresponding Author

**Ying-Song Yu** − *Department of Mechanics, School of Civil Engineering, Architecture and Environment, Hubei University of Technology, Wuhan 430068, P. R. China;* orcid.org/0000-0002-3914-1121; Email: yuys@hbut.edu.cn

### Authors

**Xiao-Ye Yang** − *Department of Mechanics, School of Civil Engineering, Architecture and Environment, Hubei University of Technology, Wuhan 430068, P. R. China*

**Guo-Hao Li** − *Department of Mechanics, School of Civil Engineering, Architecture and Environment, Hubei University of Technology, Wuhan 430068, P. R. China*

**Xianfu Huang** − *State Key Laboratory of Nonlinear Mechanics, Institute of Mechanics, Chinese Academy of Sciences, Beijing 100190, P. R. China; School of Engineering Science, University of Chinese Academy of Sciences, Beijing 100049, P. R. China;* orcid.org/0000-0002-5859-8135

Complete contact information is available at: https://pubs.acs.org/10.1021/acs.langmuir.2c01564

### Notes

The authors declare no competing financial interest.

## ACKNOWLEDGMENTS

This work was jointly supported by National Natural Science Foundation of China (Grant No. 11572114), the Chinese Academy of Sciences Key Research Program of Frontier Sciences (Grant No. QYZDJ-SSW-JSC019), and PetroChina Innovation Foundation (2019D-5007-0102).

## REFERENCES

(1) Deegan, R. D.; Bakajin, O.; Dupon, T. F.; Huber, G.; Nagel, S. R.; Witten, T. A. Capillary flow as the cause of ring stains from dried liquid drops. *Nature* **1997**, *389*, 827−829.

(2) Hu, H.; Larson, R. G. Analysis of the effects of Marangoni stresses on the microflow in an evaporating sessile droplet. *Langmuir* **2005**, *21*, 3972−3980.

(3) Zhang, J.; Sekimoto, A.; Okano, Y.; Dost, S. Numerical simulation of thermal-solutal Marangoni convection in a shallow rectangular cavity with mutually perpendicular temperature and concentration gradients. *Phys. Fluids* **2020**, *32*, 102108.

(4) Soltman, D.; Subramanian, V. Inkjet-printed line morphologies and temperature control of the coffee ring effect. *Langmuir* **2008**, *24*, 2224−2231.

(5) Cuk, T.; Troian, S. M.; Hong, C. M.; Wagner, S. Using convective flow splitting for the direct printing of fine copper lines. *Appl. Phys. Lett.* **2000**, *77*, 2063−2065.
(6) He, P.; Derby, B. Controlling coffee ring formation during drying of inkjet printed 2D inks. *Adv. Mater. Interfaces* **2017**, *4*, 1700944.
(7) Kong, Y. L.; Tamargo, I. A.; Kim, H.; Johnson, B. N.; Gupta, M. K.; Koh, T.-W.; Chin, H.-A.; Steingart, D. A.; Rand, B. P.; McAlpine, M. C. 3D printed quantum dot light-emitting diodes. *Nano Lett.* **2014**, *14*, 7017−7023.
(8) Lee, J. A.; Reibel, K.; Snyder, M. A.; Scriven, L. E.; Tsapatsis, M. Geometric model describing the banded morphology of particle films formed by convective assembly. *ChemPhysChem* **2009**, *10*, 2116−2122.
(9) Park, B.; Na, S. Y.; Bae, I.-G. Uniform two-dimensional crystals of polystyrene nanospheres fabricated by a surfactant-assisted spin-coating method with polyoxyethylene tridecyl ether. *Sci. Rep.* **2019**, *9*, 11453.
(10) Carreón, Y. J.; Ríos-Ramírez, M.; Moctezuma, R.; González-Gutiérrez, J. Texture analysis of protein deposits produced by droplet evaporation. *Sci. Rep.* **2018**, *8*, 9580.
(11) Zang, D.; Tarafdar, S.; Tarasevich, Y. Y.; Choudhury, M. D.; Dutta, T. Evaporation of a droplet: from physics to applications. *Phys. Rep.* **2019**, *804*, 1−56.
(12) Bou Zeid, W.; Brutin, D. Influence of relative humidity on spreading, pattern formation and adhesion of a drying drop of whole blood. *Colloid Surfaces A* **2013**, *430*, 1−7.
(13) Woolley, A. T.; Kelly, R. T. Deposition and characterization of extended single-stranded DNA molecules on surfaces. *Nano Lett.* **2001**, *1*, 345−348.
(14) Dugas, V.; Broutin, J.; Souteyrand, E. Droplet evaporation study applied to DNA chip manufacturing. *Langmuir* **2005**, *21*, 9130−9136.
(15) Sharma, R.; Strano, M. S. Centerline placement and alignment of anisotropic nanotubes in high aspect ratio cylindrical droplets of nanometer diameter. *Adv. Mater.* **2009**, *21*, 60−65.
(16) Xia, D.; Brueck, S. Strongly anisotropic wetting on one dimensional nanopatterned surfaces. *Nano Lett.* **2008**, *8*, 2819−2824.
(17) Vakarelski, I. U.; Chan, D. Y.; Nonoguchi, T.; Shinto, H.; Higashitani, K. Assembly of gold nanoparticles into microwire networks induced by drying liquid bridges. *Phys. Rev. Lett.* **2009**, *102*, 058303.
(18) Mampallil, D.; Eral, H. B. A review on suppression and utilization of the coffee-ring effect. *Adv. Colloid Interface Sci.* **2018**, *252*, 38−54.
(19) Dicuangco, C.; Dash, S.; Weibel, J. A.; Garimella, S. V. Effect of superhydrophobic surface morphology on evaporative deposition patterns. *Appl. Phys. Lett.* **2014**, *104*, 201604.
(20) Cui, L.; Zhang, J.; Zhang, X.; Li, Y.; Wang, Z.; Gao, H.; Wang, T.; Zhu, S.; Yu, H.; Yang, B. Avoiding coffee ring structure based on hydrophobic silicon pillar arrays during single-drop evaporation. *Soft Matter* **2012**, *8*, 10448−10456.
(21) Eral, H. B.; Mampallil, A. D.; Duits, M. H. G.; Mugele, F. Suppressing the coffee stain effect: How to control colloidal self-assembly in evaporating drops using electrowetting. *Soft Matter* **2011**, *7*, 4954−4958.
(22) Bhardwaj, R.; Fang, X. H.; Somasundaran, P.; Attinger, D. Self-assembly of colloidal particles from evaporating droplets: Role of DLVO interactions and proposition of a phase diagram. *Langmuir* **2010**, *26*, 7833−7842.
(23) Ristenpart, W. D.; Kim, P. G.; Domingues, C.; Wan, J.; Stone, H. A. Influence of substrate conductivity on circulation reversal in evaporating drops. *Phys. Rev. Lett.* **2007**, *99*, 234502.
(24) Parsa, M.; Harmand, S.; Sefiane, K.; Bigerelle, M.; Deltombe, R. Effect of substrate temperature on pattern formation of nanoparticles from volatile drops. *Langmuir* **2015**, *31*, 3354−3367.
(25) Majumder, M.; Rendall, C. S.; Eukel, J. A.; Wang, J. Y. L.; Bahabtu, N.; Pint, C. L.; Liu, T. Y.; Orbaek, A. W.; Mirri, F.; Nam, J.; Barron, A. R.; Hauge, R. H.; Schmidt, H. K.; Pasquali, M. Overcoming the "coffee-stain" effect by compositional Marangoni-flow-assisted drop-drying. *J. Phys. Chem. B* **2012**, *116*, 6536−6542.
(26) Zhang, Y. J.; Liu, Z. T.; Zang, D. Y.; Qian, Y. M.; Lin, K. J. Pattern transition and sluggish cracking of colloidal droplet deposition with polymer additives. *Sci. China Phys. Mech. Astron.* **2013**, *56*, 1712−1718.
(27) Marin, A.; Liepelt, R.; Rossi, M.; Kähler, C. J. Surfactant-driven flow transitions in evaporating droplets. *Soft Matter* **2016**, *12*, 1593−1600.
(28) Kovalchuk, N. M.; Matar, O. K.; Craster, R. V.; Miller, R.; Starov, V. M. The effect of adsorption kinetics on the rate of surfactant-enhanced spreading. *Soft Matter* **2016**, *12*, 1009−1013.
(29) Bzdek, B. R.; Reid, J. P.; Malila, J.; Prisle, N. L. The surface tension of surfactant-containing, finite volume droplet. *Proc. Natl. Acad. Sci. U.S.A.* **2020**, *117*, 8335−8343.
(30) Still, T.; Yunker, P. J.; Yodh, A. G. Surfactant-induced Marangoni eddies alter the coffee-rings of evaporating colloidal drops. *Langmuir* **2012**, *28*, 4984−4988.
(31) Saxena, N.; Naik, T.; Paria, S. Organization of SiO2 and TiO2 nanoparticles into fractal patterns on glass surface for the generation of superhydrophilicity. *J. Phys. Chem. C* **2017**, *121*, 2428−2436.
(32) Inanlu, M. J.; Shojaan, B.; Farhadi, J.; Bazargan, V. Effect of particle concentration on surfactant-induced alteration of the contact line deposition in evaporating sessile droplets. *Langmuir* **2021**, *37*, 2658−2666.
(33) Nassar, N. N.; Cortés, F. B.; Franco, C. A. *Nanoparticles: an emerging technology for oil production and processing applications*; Springer Nature: Switzerland AG, Cham, 2021. Switzerland, 2021.
(34) Kwieciński, W.; Segers, T.; van der Werf, S.; van Houselt, A.; Lohse, D.; Zandvliet, H. J. W.; Kooiu, S. Evaporation of dilute sodium dodecyl sulfate droplets on a hydrophobic substrate. *Langmuir* **2019**, *35*, 10453−10460.
(35) Nakahara, H.; Shibata, O.; Rusdi, M.; Moroi, Y. Examination of surface adsorption of soluble surfactants by surface potential measurement at the air/solution interface. *J. Phys. Chem. C* **2008**, *112*, 6398−6403.
(36) Yang, Y. J.; Corti, D. S.; Franses, E. I. Effect of Triton X-100 on the stability of titania nanoparticles against agglomeration and sedimentation: a masked depletion interaction. *Colloid Surf. A* **2017**, *516*, 296−304.
(37) Basu, N.; Mukherjee, R. Morphology modulation in evaporative drying mediated crystallization of sodium chloride solution droplet with surfactant. *Soft Matter* **2018**, *14*, 7883−7893.
(38) Yu, Y. S.; Zhu, Y. Q.; Huang, X. F.; Zhou, J. Z.; Zhou, A. Effect of substrate elasticity on evaporation kinetics and evaporative deposition of aqueous polystyrene nanoparticles droplets. *Sci. China Phys. Mech. Astron.* **2020**, *63*, 114612.
(39) Goehring, L.; Clegg, W. J.; Routh, A. F. Wavy cracks in drying colloidal films. *Soft Matter* **2011**, *7*, 7984−7987.
(40) Man, W.; Russel, W. B. Direct measurements of critical stresses and cracking in thin films of colloid dispersions. *Phys. Rev. Lett.* **2008**, *100*, 198302.
(41) Xu, Y.; German, G. K.; Mertz, A. F.; Dufresne, E. R. Imaging stress and strain in the fracture of drying colloidal films. *Soft Matter* **2013**, *9*, 3735.
(42) Schneider, M.; Maurath, J.; Fischer, S. B.; Weiss, M.; Willenbacher, N.; Koos, E. Suppressing crack formation in particulate systems by utilizing capillary forces. *ACS Appl. Mater. Interfaces* **2017**, *9*, 11095−11105.
(43) Tirumkudulu, M. S.; Russel, W. B. Cracking in drying latex films. *Langmuir* **2005**, *21*, 4938−4948.
(44) Lohani, D.; Basavaraj, M. G.; Satapathy, D. K.; Sarkar, S. Coupled effect of concentration, particle size and substrate morphology on the formation of coffee rings. *Colloid Surface A* **2020**, *589*, 124387.
(45) Kralchevsky, P. A.; Nagayama, K. Capillary interactions between particles bound to interfaces, liquid films and biomembranes. *Adv. Colloid Interface Sci.* **2000**, *85*, 145−192.


https://doi.org/10.1021/acs.langmuir.2c01564
*Langmuir* 2022, 38, 11666−11674

(46) Kralchevsky, P. A.; Denkov, N. D. Capillary forces and structuring in layers of colloid particles. *Curr. Opin. Colloid Interface Sci.* **2001**, *6*, 383−401.
(47) Nikolov, A. D.; Wasan, D. T. Mechanisms of the assembly of nano- and microparticle two-dimensional structures in a wedge film. *Ind. Eng. Chem. Res.* **2009**, *48*, 2320−2326.
(48) Li, W. B.; Lan, D.; Wang, Y. R. Dewetting-mediated pattern formation inside the coffee ring. *Phys. Rev. E* **2017**, *95*, 042607.
(49) Divry, V.; Jacomine, L.; Le Houérou, V.; Collin, D.; Gauthier, C.; Holl, Y. Influence of formulation on friction properties of latex films. *Proc. Org. Coat.* **2017**, *113*, 189−199.
(50) Lee, B.; Yu, Y. H.; Cho, D. S.; Cho, Y. J. Role of additive concentration in slow-speed sliding contact under boundary lubrication conditions. *J. Mater. Sci. Technol.* **2019**, *33*, 5361−5368.
(51) Chhasatia, V. H.; Sun, Y. Interaction of bi-dispersed particles with contact line in an evaporating colloidal drop. *Soft Matter* **2011**, *7*, 10135−10143.
(52) Jung, J. Y.; Kim, Y. W.; Yoo, J. Y.; Koo, J.; Kang, Y. T. Forces acting on a single particle in an evaporating sessile droplet on a hydrophilic surface. *Anal. Chem.* **2010**, *82*, 784−788.
(53) Karapetsas, G.; Sahu, K. C.; Matar, O. K. Evaporation of sessile droplets laden with particles and insoluble surfactants. *Langmuir* **2016**, *32*, 6871−6881.
(54) Zhang, Y. J.; Qian, Y. M.; Liu, Z. T.; Li, Z. G.; Zang, D. Y. Surface wrinkling and cracking dynamics in the drying of colloidal droplets. *Eur. Phys. J. E* **2014**, *37*, 84.
(55) Lama, H.; Basavaraj, M. G.; Satapathy, D. K. Tailoring crack morphology in coffee-ring deposits via substrate heating. *Soft Matter* **2017**, *13*, 5445−5452.





https://doi.org/10.1021/acs.langmuir.2c01564
*Langmuir* 2022, 38, 11666−11674